Monitoring Variations in Thermal Curing of Nanoparticle Coatings
through Confocal Raman Microscopy and Principal Component Analysis
Peer-reviewed author version

Monitoring variations in thermal curing of nanoparticle coatings through confocal Raman microscopy and principal component analysis
--Manuscript Draft--

Manuscript Number:	pssa.201900651R2
Article Type:	Original Paper
Corresponding Author:	Pieter Samyn, Dr. Universiteit Hasselt Hasselt, BELGIUM
Corresponding Author E-Mail:	pieter.samyn@uhasselt.be
Order of Authors:	Pieter Samyn, Dr.
	Wouter Marchal
	Dries Vandamme
	Peter Adriaensens
	Robert Carleer
Keywords:	coating, surface characterization, Raman spectroscopy, mapping, statistical analysis
Section/Category:	Engineering of Functional Interfaces (EnFI 2019)
Abstract:	For paper coatings with organic nanoparticles of poly(styrene- co -maleimide), the dispersive Raman spectroscopy and confocal Raman microscopy are applied for a qualitative and quantitative analysis of the lateral distribution of chemical moieties as a function of different coating grades (degree of imidization) and thermal curing temperatures (120 to 250°C). The Raman mapping with band intensity ratios, single band intensities and average spectral intensities illustrates that surface locations with imide moieties are sensitive to the thermal curing temperature due to the reactivity of an amount ammonolyzed (non-imidized) maleic anhydride, while the styrene moieties are not sensitive to the thermal curing. A maximum in imide functionalities at the surface occurs after curing at 135 to 150°C depending on the coating grade. The surface coverage of the coating moieties are complementary to the cellulose components, but local variations in specific Raman bands for the latter suggest interactions due to hydrogen bonding. The principal component analysis with two parameters allows for a good quantification of the imide content and surface coverage.
Author Comments:	
Additional Information:	
Question	Response
Please submit a plain text version of your cover letter here.	Dear editor, In response to my participation in the EnFi 2019 workshop in Leuven (Belgium), I would be happy to contribute a paper about the presented research poster within the special issue of PPS a dedicated to this workshop. This paper contains original experimental data on the Raman spectroscopy and chemical imaging of functional coatings on paper and the contained data with the experimental matrix has not been presented before. The use of Raman spectroscopy is an important analytical tool for evaluation of functional surfaces and interfaces and is here presented as a case study on a specific coating system on paper substrates. The coatings can be used as hydrophobic surface modification, but the emphasis of this research paper lies into an in-depth analytical evaluation of data obtained from Raman analysis.

	We hope that the paper can be considered for the special issue and we are looking forward to receive further instructions with reviewer reports. With best regards Pieter Samyn.
Do you or any of your co-authors have a conflict of interest to declare?	No. The authors declare no conflict of interest.
Response to Reviewers:	

WILEY-VCH

Monitoring variations in thermal curing of nanoparticle coatings through confocal Raman microscopy and principal component analysis

Pieter Samyn,* Wouter Marchal, Dries Vandamme, Peter Adriaensens, and Robert Carleer

Dr. ir. P. Samyn, Prof. Dr. W. Marchal, Prof. Dr. ir. D. Vandamme, Prof. Dr. P. Adriaensens, Prof. Dr. R. Carleer

University of Hasselt, Institute for Materials Research (IMO-IMOMEC), Applied and Analytical Chemistry
Agoralaan Gebouw D, B-3590 Diepenbeek, Belgium.
E-mail: pieter.samyn@uhasselt.be

Keywords: coating, surface characterization, Raman spectroscopy, mapping, chemometrics

For paper coatings with organic nanoparticles of poly(styrene-*co*-maleimide), the dispersive Raman spectroscopy and confocal Raman microscopy are applied for a qualitative and quantitative analysis of the lateral distribution of chemical moieties as a function of different coating grades (degree of imidization) and thermal curing temperatures (120 to 250°C). The Raman mapping with band intensity ratios, single band intensities and average spectral intensities illustrates that surface locations with imide moieties are sensitive to the thermal curing temperature due to the reactivity of an amount ammonolyzed (non-imidized) maleic anhydride, while the styrene moieties are not sensitive to the thermal curing. A maximum in imide functionalities at the surface occurs after curing at 135 to 150°C depending on the coating grade. The surface coverage of the coating moieties are complementary to the cellulose components, but local variations in specific Raman bands for the latter suggest interactions due to hydrogen bonding. The principal component analysis with two parameters allows for a good quantification of the imide content and surface coverage.

1. Introduction

The creation of functional surfaces with specific response to external stimuli or interaction with the environment often relies on the introduction of specific chemical moieties at the surface. The changes in local chemical surface composition may intentionally be introduced by means of wet-chemical surface modification and/or coating deposition. Among different applications, the adaptation and control of chemical surface properties is required for control of wetting,[1] adsorption, [2] bacterial biofilm formation,[3] bacterial and algae interaction,[4] adhesive bonding,[5] cell adhesion and growth,[6] lubrication,[7] etc. Many of the mechanisms controlling the surface properties are mimicked from nature and/or biological materials,[8] and are intensified in combination with the introduction of a nanostructure topography at the surface.[9] In particular, the deposition of hydrophobic nanoparticles allows to create hydrophobic to super-hydrophobic surfaces.[10]

The interest in surface engineering of paper substrates has grown in respect to the demand for eco-friendly, recyclable and low-cost substrates. The functionality of cellulose fibers with abundance of hydroxyl groups particularly offers a broad platform for surface modification. For primary use as a packaging material or as a printing substrate, the open structure of a paper web has to be covered with multiple coating layers to provide water repellence, oil and grease resistance, or gas barrier properties. The chemical modification of paper surfaces through chemical grafting (e.g., for colorimetric and optical detection)[11], or by deposition of nanoparticles (e.g. for colorimetric sensing of chemicals)[12] has become an emerging field of research in order to create targeted properties or operating devices. The functionalization of papers for antibacterial and antimicrobial resistance against bacteria, fungi and algae utilizes metallic and/or oxide nanoparticles.[13] The surface properties for photo-active papers can be enhanced by deposition of metallic nanoparticles.[14] A broad variety of coating materials includes inorganic and organic nanoparticles as reviewed before for food packaging,[15] to improve its performance towards lotus-like paper/paperboard.[16] Most interestingly, the hydrophobic paper coatings can be formed with non-toxic organic nanoparticles, such as esterified lignin particles,[17] cellulose particles with stearic acid,[18] polyhydroxybutyrate particles,[19] or wax-filled core-shell particles.[20] Overall, the creation of a fully protective hydrophobic layer with nanoparticles onto the hydrophilic cellulose fibers requires a homogeneous surface coverage and good control over the local presentation of specific hydrophobic functional groups within the outer coating layer. In particular, the conditions of a thermal heat curing treatment on soft coatings may further affect the morphology and chemical

surface composition, due to mechanisms of migration, polymerization, cross-linking, visco-elastic flow or degradation, with consequent effects on barrier coating performance.[21]

In parallel with the creation of functional surfaces by chemical modification, the use of proper analytical evaluation tools and interpretation of analytical data should provide better insight in relationships between coating compositions and surface characteristics. Besides several techniques used for paper surface analysis, such as XPS (X-ray photoelectron spectroscopy),[22] or SIMS (secondary ion mass spectroscopy),[23] the Raman spectroscopy is frequently applied in studies of paper and paper coating surfaces. The current state and recent developments in surface analysis for paper and coatings and specific use of Raman spectroscopy has been reviewed before.[24] The confocal Raman microscopy is a non-destructive tool that allows for chemical imaging,[25] which includes spatial information for the quantification of different substrates and is frequently used as an analytical tool for quality control,[26] or understanding of coating distribution, defects and failure.[27] The Raman mapping is often combined with chemometric analysis, where principal component analysis (PCA) may be more accurate than univariate methods in case of polymer curing.[28] In particular, the compositional mapping of paper coatings is able to give the spatial distribution of main coating components such as kaolin, anatase, styrene butadiene, ground calcium carbonate and precipitated calcium carbonate.[29] The confocal Raman spectroscopy can successfully discriminate between the main components of a coating formulation (pigments, binders and additives) and the spectra show characteristic fingerprint patterns for the raw materials with an indication of their spatial distribution in submicron ranges.[30] The presence of starch in 1 to 2 wt.-% in paper cross sections could be quantitatively monitored by Raman microscopy and better distinguished by use of principal component analysis.[31] The migration of certain ingredients during coating application resulting in various surface compositions can be followed as a function of the particle size.[32] By proper adaption of the laser and detector conditions, Raman spectroscopy was introduced as an on-line tool with good resolution/bandwidth and alleviating the contradiction between sample fluorescence and detector response.[33] The lateral mapping of styrene-butadiene latex coatings provided good insight in the spatial distribution of the chemical compounds within a coating relatively to the paper substrate.[34] The Raman spectra are sensitive to relatively low concentrations for paper and coating additives with a relatively high spectral resolution, but it seems more difficult to differentiate between minor coating additives such as rheological modifiers, nanoparticles or dispersants. In addition, major deficiencies in the use of Raman spectroscopy for paper coating analysis include the presence of non-uniform morphologies of the substrate.

In this study, the variations in lateral distribution of chemical moieties within paper coatings containing organic nanoparticles have been investigated by Raman spectroscopy and confocal Raman microscopy in order to get qualitative and quantitative data on the variation in chemical surface composition as a function of the coating grade and thermal curing temperature. Through the use of principal component analysis, the surface coverage and homogeneity of the coating on a paper substrate was further quantified. The monitoring of the thermal curing effects on the chemical reactivity of an organic coating allows for an optimization of the curing conditions resulting in a maximum surface coverage and content of hydrophobic moieties at the surface. In particular, the possibility for tuning the surface chemistry of the coating depending on thermal curing conditions is an interesting way for creating surfaces with adjustable surface functionality and in-situ control of the surface composition.

2. Experimental Section

2.1. Materials

The coating materials were available as aqueous dispersions of poly(styrene-*co*-maleimide) or SMI nanoparticles that were imidized from a precursor of the poly(styrene-*co*-maleic anhydride) or SMA copolymer with a molecular weight M_w = 80.000 g/mol. Different grades of the SMI nanoparticle coating materials were included in this study, starting from SMA precursors of increasing molar percentages of maleic anhydride (MA) and complementary percentage of styrene (St), i.e. 26 mol-% MA, 74 mol-% St (SMI-26); 28 mol-% MA, 72 mol-% St (SMI-28); 33 mol-% MA, 67 mol-% St (SMI-33); and 34 mol-% MA, 66 mol-% St (SMI-34). The commercial grades of SMA copolymers were obtained from Polyscope (Geleen, The Netherlands). The conversion of the reactive maleic anhydride groups into imide groups was done by a two-step process, including (i) ammonolysis or ring-opening of the MA at temperatures of 80 to 100°C, and (ii) imidization or ring-closing reaction of the ammonolysed MA at temperatures of 140 to 160°C. An appropriate degree of imidization per SMI grade was obtained after preliminary selection of appropriate temperature and reaction time,[35] with a certain amount of remaining ammonolyzed MA accounting for the good stability of the SMI nanoparticle dispersions. In practice, the imidization of SMA was done in presence of ammonium hydroxide and water in a ratio of ammonium relatively to the maleic anhydride of NH₃/MA = 1.01 and reaction temperature of 160°C. The SMA pellets were obtained as white pellets and crushed in the required amount for a single batch reaction, i.e. typically 240 g of a given SMA grade was loaded with a fixed volume of 700 ml water and 190 ml of a 25 %

aqueous ammonium hydroxide solution. The reaction was performed by charging the materials in a 1 liter autoclave reactor under continuous stirring with anchor stirrer at a speed of 400 rpm during a reaction time of about 300 min under a constant pressure of 6 bar. After cooling down the reactor during about 30 minutes, an aqueous nanoparticle dispersion was obtained for the different SMI grades with good homogeneity and no agglomerates. The further details on material synthesis and SMI nanoparticles characteristics can be found in a previous report:[35] in summary, the physico-chemical properties of the SMI nanoparticle dispersions used for coating deposition are given in **Table 1.** All coating dispersions show good stability with Zetapotential between -50 to -60 mV, maximum solid content at around 35 wt.-% and gradually increasing viscosity depending on the imide content. The viscosity is influenced by the remaining fraction of ammonolyzed MA and increases with the higher MA grade in parallel with a lower pH-value.[35]

Table 1. Physico-chemical characteristics of coating materials as aqueous dispersion

Coating grade	pH	Zetapotential [mV]	Solid content [wt.-%]	Viscosity [cP]	z-average mean size [nm]	Polydispersity
SMI-26	6.8	- 60	35.9	176	85	0.21
SMI-28	6.7	- 58	34.6	664	91	0.23
SMI-33	5.3	- 55	35.3	720	109	0.23
SMI-34	5.2	- 52	27.8	892	197	0.24

2.2 Coating application and thermal curing

The aqueous SMI nanoparticle dispersions as prepared were deposited as a coating onto a standard copy paper grade (Mondi Business Paper, 100 g/m^2, thickness 125 μm) by using a laboratory-scale bar coater K303 multi-coater (RK Print Coat Instruments Ltd., UK) with a standard metering bar number 3 characterized by close wire-wound diameter 0.30 mm. An A4 size of the paper was clamped onto the coating table and a fixed bar speed of 6 mm/s under controlled pressure in contact with the paper surface was selected. A given volume of the SMI dispersion was manually applied near the metering bar by using a 10 ml pipet and the bar movement was parallel to the machine direction (MD) of the paper. After coating deposition, the samples were dried for 2 min at 120°C in a circulating hot-air oven where the short drying time allows to remove the contained water. The dried coatings were subsequently stored for 1 week under controlled environmental conditions (23°C, 60 % RH) before they were further processed. The wet coating thickness was calculated to be about 24 ± 2 μm and verified by experimental measurements (ASTM D4414). The dry coating thickness was evaluated by

The thermal curing of the coatings was subsequently done in a circulating hot-air oven by placing the coated paper samples in a pre-heated oven at different temperatures of 125, 135, 150, 180, 220 and 250°C for a given time of 6 hours. After removal of the samples from the oven, they were cooled under room conditions and stored for 1 day under controlled environmental conditions (23°C, 60% RH) until further characterization. The top-surface morphology of the resulting paper coating after deposition and thermal curing at different temperatures is illustrated in **Figure 1** by scanning electron microscopy (Tabletop TM3000, Hitachi, Krefeld, Germany).
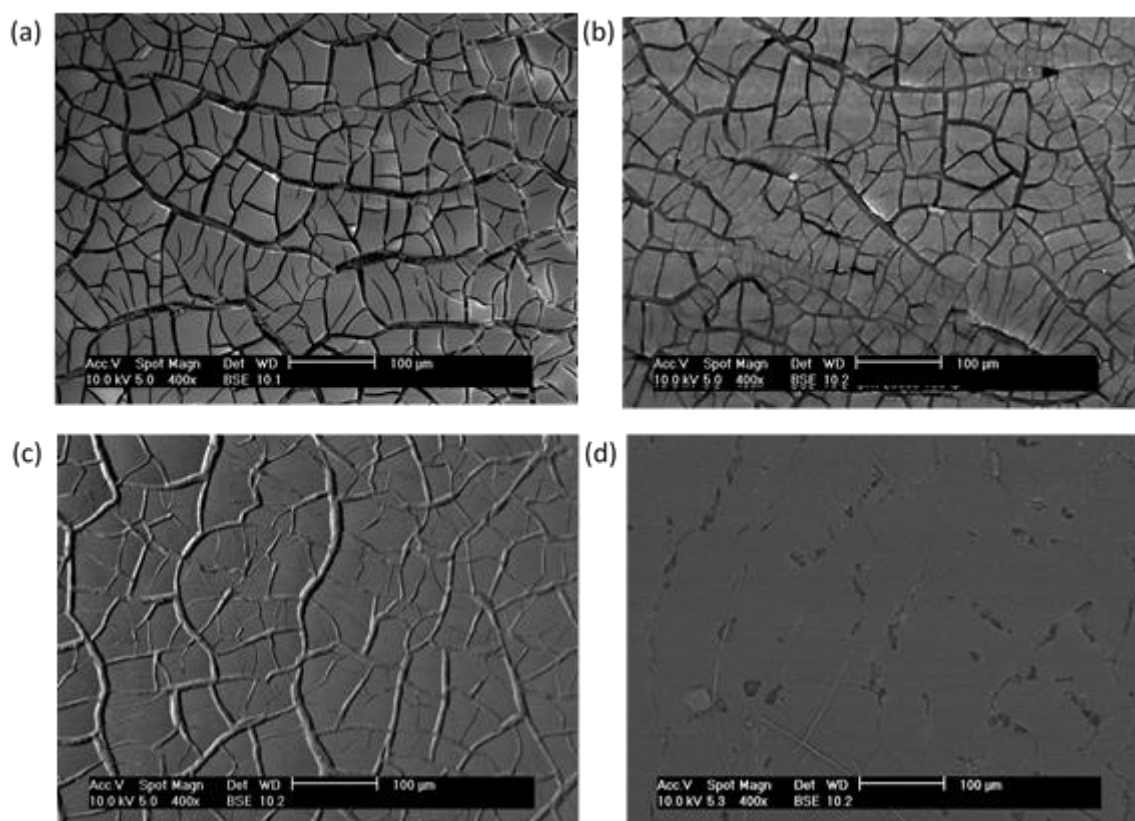

Figure 1. Scanning electron microscopy showing morphology of studied coatings of SMI-26 on paper substrate, (a) uncured, and thermally cured at (b) 135°C, (c) 180°C, (d) 250°C.

6

2.3 Analytical techniques

The Raman spectra were collected as top views on the coated paper surfaces (papers glued onto a microscopic glass slide), by using a Raman Flex 400 station (Perkin Elmer, Rodgau, Germany) connected to a Raman micro 300 station and confocal BX51 optical microscope (Olympus, Hamburg, Germany) with motorized XYZ sampling stage. The laser wavelength of 785 nm was operated at a power of 40 mW (at sample position) and guided through an objective lens with magnification of 20 x (numerical aperture = 0.40, pinhole size = 50 μm), with a measuring time of 10 s and 6 exposures per point while refocusing of the laser spot (2 μm spot diameter) at each measuring point on the surface in order to correct for local variations in surface height. The penetration depth of the laser beam for the present system was calculated at 5 μm by using the Beer-Lambert Law assuming a refractive index of 1.5 and laser wavelength of 785 nm. The surface maps with area of 1 x 1 mm^2 were recorded as an array of 20 x 20 measuring points with a 0.05 mm interdistance, with interpolation of data between the single measuring points. The spectra were recorded in the range of 3200 to 200 cm^{-1} with a resolution of 4 cm^{-1} through a dispersive system with multichannel CCD array detector that is cooled at -50°C, incorporating a 1024 x 256 pixel sensor. The commercial software of Spectrum Image (version R1.7, Perkin Elmer) was used for data processing of the surface maps with band ratio intensities, single bands and average (or integrated) intensities. A baseline correction was performed by selecting fixed baseline points in all spectra (e.g. 3500, 3140, 2790, 1800, 1670, 1520, 1220, 938, 860, 675, 460 cm-1), allowing for isolation of specific spectral bands or group of bands that correlate to imide, styrene or cellulose. The spectra were consequently normalized on the styrene band at 1600 cm^{-1}, as the latter styrene groups are expected to be inert during thermal curing.

The principal component analysis (PCA) was performed by using Unscrambler 10.1 software (Camo Analytics, Oslo, Norway). The statistical model was built from 10 independent Raman spectra per sample (including original coated papers and thermally cured papers) that were collected at independent and random places over the surface of a single coated paper with size of 5 x 5 cm^2. The data sets for PCA include Raman spectra with full spectral range (3200 to 200 cm^{-1}) that were first processed by previously named baseline correction and normalization. A cross-validation of the calibration set was consequently done by leaving out one of the calibration samples from the regression model and verifying the model for the remaining samples. Finally, a new and independent data-set of Raman spectra collected at five positions on new coated paper samples (used SMI dispersions from the same batch) was used as an external validation test of the statistical PCA model.

3. Results and Discussion

3.1 Raman spectroscopy

The Raman spectra of coated papers after thermal curing at different temperatures are shown in **Figure 2**, with an indication of the main bands in the fingerprint region to be considered in present study. As a reference, the Raman spectrum of the uncoated base paper includes characteristic cellulose bands at 1470 cm^{-1} (H-C-H bending), 1456 cm^{-1} (H-O-C bending), 1409 cm^{-1} (H-C-C bending), 1378 cm^{-1} (H-C-O bending), 1340 cm^{-1} (H-O-C bending), 1292 and 1152 cm^{-1} (H-C-C and H-C-O bending), 1120, 1084, 1063, 1037, 997 cm^{-1} (H-C-C and H-C-O stretching), 1120 (C-O-C symmetrical stretching) and 1095 cm^{-1} (C-O-H asymmetrical stretching). The characteristic Raman bands for cellulose were assigned before,[36] and are clearly represented in the coated paper substrates, as the calculated penetration depth of the Raman signal under present experimental conditions is about 5 µm when using an objective of 20 x and refractive index of 1.5, while the coating thickness is about 2 µm. The additional Raman bands are associated with the coating moieties of imide at 1785 cm^{-1} (imide I, C=O) and styrene at 1602 cm^{-1} (aromatic skeletal ring stretching), 1583 cm^{-1} (aromatic C=C stretching), 1452 cm^{-1} (C-H$_2$ scissoring), 1183 cm^{-1} (C-H, C-C aromatic stretching), 1031 cm^{-1} (C-H in-plane deformation) and 1000 cm^{-1} (aromatic ring breathing mode), 795 cm^{-1} (C-H out-of-plane deformation). The characteristic Raman bands for imide,[37] and styrene,[38] are well represented in the spectra. The baseline correction and normalization procedures on the 1600 cm^{-1} styrene band as described, equally resulted in a constant styrene band near 1000 cm^{-1}. In contrast, variations in the imide regions and cellulose regions for baseline corrected and normalized spectra were noticed after thermal curing.

As illustrated for the SMI-26 coatings, a single representative spectrum of the paper coating is selected after curing at different temperatures (overview of stacked spectra in main graph and detail with overlay spectra in right inset **Figure 2**), together with a reference spectrum of uncoated paper. A variation in the intensity of the imide band at 1785 cm^{-1} relatively to a constant intensity of the styrene band at 1602 cm^{-1} can be noticed upon thermal curing: the imide band grows towards maximum intensity between 125 and 135°C and diminishes at higher temperatures of 150 to 250°C. In more detail, the region of the imide I band at 1785 cm^{-1} contains a shoulder band at 1780 cm^{-1} representing the anhydride C=O moieties related to the poly(styrene-*co*-maleic anhydride) or SMA copolymer used as a precursor for the imidization. At the temperature of maximum imide I intensity of 125 to 135°C, the anhydride C=O shoulder band disappears while it remains visible at lower temperatures (due to incomplete imidization) and reappears at higher temperatures (due to reversible degradation of the imide structure). The

degradation of poly(styrene-*co*-maleimide) at highest temperatures of 250°C can equally be noticed by prevalent intensification of Raman bands at 772 cm^{-1} (aromatic ring breathing) due to monomeric styrene, and Raman bands at 1520 cm^{-1} (carboxylic C=O) due to amic acid formation. The band at 1520 cm^{-1} is due to the presence of amide II (NH bending + CN stretching) and can be related to intermediate products formed during the imidization of the poly(styrene-*co*-maleic anhydride) precursor, which involves the ring-opening of the maleic anhydride structure of the SMA precursor in presence of ammonium hydroxide and formation of ammonolyzed maleic anhydride. In parallel, the Raman band at 1800 cm^{-1} (C=O carboxylic acid) appears slightly at 125, 180 and 250°C and disappears at temperatures of 125 to 135°C due to a maximum intensity of the imidization reaction at those temperatures. The variations in imide I band at 1785 cm^{-1} for the different coating grades SMI-26, SMI-28, SMI-33, SMI-34 (detail in left inset **Figure 2**) similarly increases with the higher imide grade relatively to a constant intensity of the styrene band.
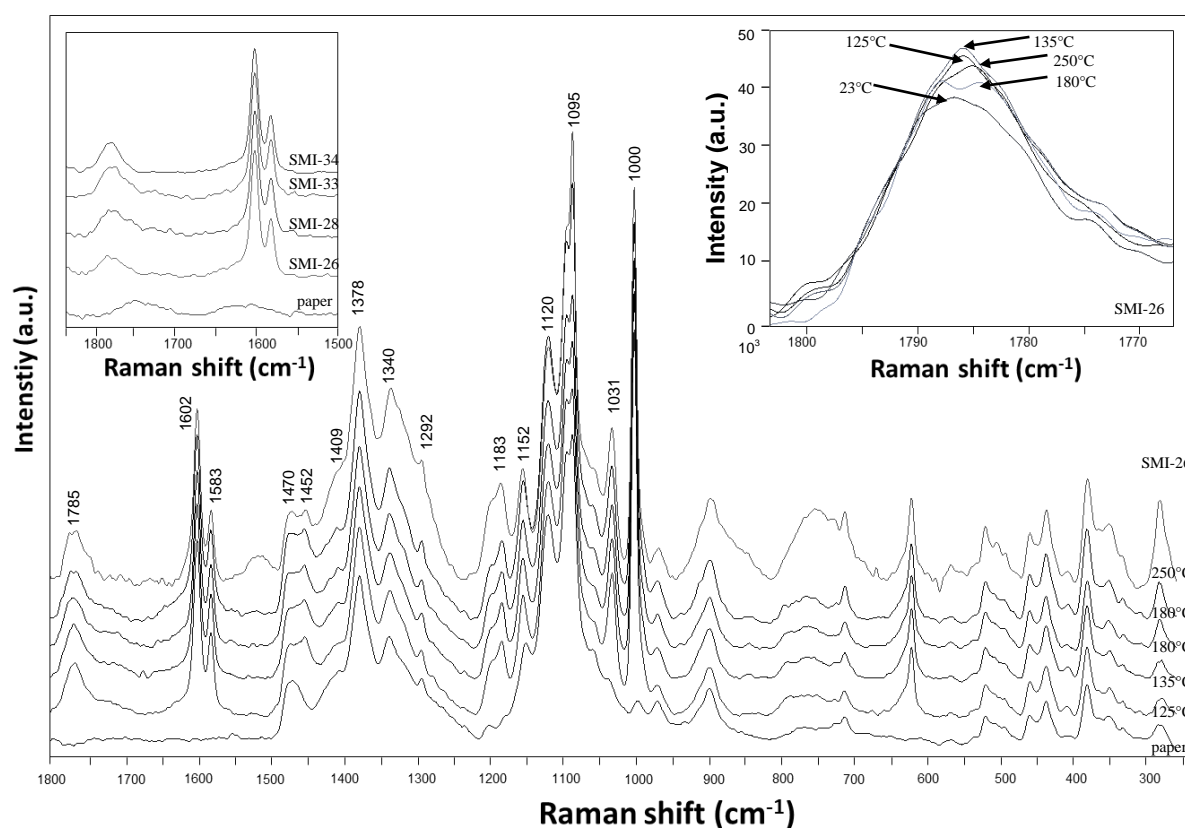

Figure 2. Raman spectra of SMI-26 coatings after thermal curing at different temperatures (main graph) with detail on the Raman band at 1785 cm^{-1} at different temperatures for SMI-26 (right inset) and detail on the Raman bands at 1785 cm^{-1} and 1602 cm^{-1} for different coating grades on original non-cured coatings (left inset).

9

3.2 Raman surface mapping

The chemical surface maps of coated papers were collected on 1 x 1 mm^2 surface areas (top surface views) for SMI-26, SMI-28, SMI-33, SMI-34 coating grades in order to study the lateral distribution of chemical moieties at the surface and surface coverage. The surface maps are systematically studied as a function of coating grade and thermal curing temperatures to evaluate trends in surface coverage, local presentation of imide and styrene moieties and relative intensity variation. A comparison will be made of the information obtained from surface maps collected as band intensity ratios, single bands, band region analysis and average intensity. The surface maps of specific band intensity ratios related to imide, styrene and cellulose are first evaluated: the styrene band was selected as a reference band to image the distribution of imide functionality within the coating itself, while the cellulose band was used as a reference band to image the coating coverage over the paper substrate. As shown in **Figure 3**, the variations in intensity of imide moieties within the coating are represented by the band intensity of imide (1785 cm^{-1}) relatively to styrene (1602 cm^{-1}). As all surface maps were calibrated onto the same intensity scale (blue = low, to red = high), a relative comparison between the different samples can be made. The surface maps indicate a homogeneous distribution of the imide moieties over the surface without macroscale coating defects or imperfections. It seems that relatively small variations in surface composition depending on the coating grade and thermal curing temperature can be sensitively monitored. There is a gradual increase in imide intensity for the different SMI coati*ng grades from SMI-26, to SMI-28, to SMI-33 and to SMI-34, which is valid for the non-cured as well as for the thermally cured coatings. This reflects the influence of the selected coating grades with consistent increase in imide content. The influence of thermal curing temperature on imide intensity of the coatings shows similar trends for all coating grades towards a maximum imide intensity at 135°C for the SMI-26 and SMI-28 coating grades, and a maximum imide intensity at 150°C for the SMI-33 and SMI-34 coating grades. At the higher temperatures of 180 to 250°C, the imide intensity lowers relatively to the maximum intensity at 135°C, while it becomes more homogeneously distributed over the surface in contrast to the often very local high intensity of imide coverage at room temperature and after curing at low temperatures. The more continuous coverage of imide functionalities observed in chemical surface maps at high temperatures, as indicated by a more continuous coverage of yellow to red color rather than very high local intensities, is in agreement with the previous morphological observations from SEM indicating flattening and coating homogenization.
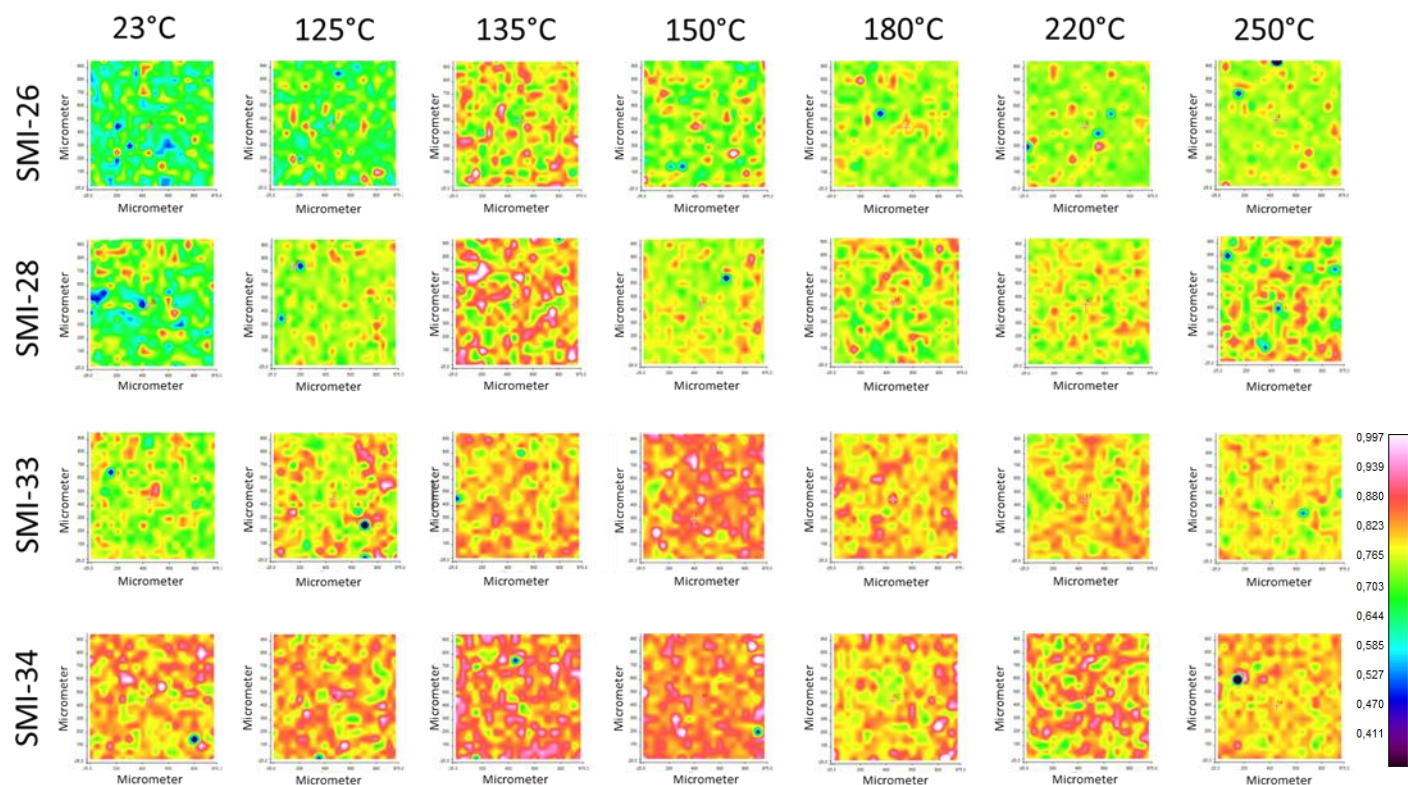
Figure 3. Raman surface maps (1 x 1 mm^2) for different SMI coating grades after thermal curing at different temperatures: band intensity ratio of imide (1785 cm^{-1}) / styrene (1602 cm^{-1}). Same intensity scale applies to all surface maps.

The coating coverage over the paper substrate is represented by the band intensity ratio of imide (1785 cm^{-1}) relatively to cellulose (1378 cm^{-1}) in **Figure 4a**, or the band intensity ratio of styrene (1602 cm^{-1}) relatively to cellulose (1378 cm^{-1}) in **Figure 4b.** It is important to notice consistent trends in surface coverage and intensities for coating moieties as a function of coating grade and thermal curing temperature. There is a good overlap in surface coverage monitored in both imide and styrene moieties that belong to the locations with coating deposits: the local maxima in imide intensity correspond to high styrene intensities, while the locations with lower intensities in both imide and styrene moieties likely correspond to thinner coating deposits. In parallel, the imide intensities consistently increase with coating grade from SMI-26 to SMI-34, while the styrene intensities consistently decrease with coating grades. The coverage with imide moieties and intensity of imide moieties per coating grade depends on the temperature. In contrast, the coverage and intensity of styrene moieties are less sensitive to the thermal curing conditions, i.e. the styrene intensities change with coating grade and remain almost constant after thermal curing as they are more inert to chemical changes upon thermal curing. The maxima in styrene intensities gradually decrease with coating grade: although slight differences
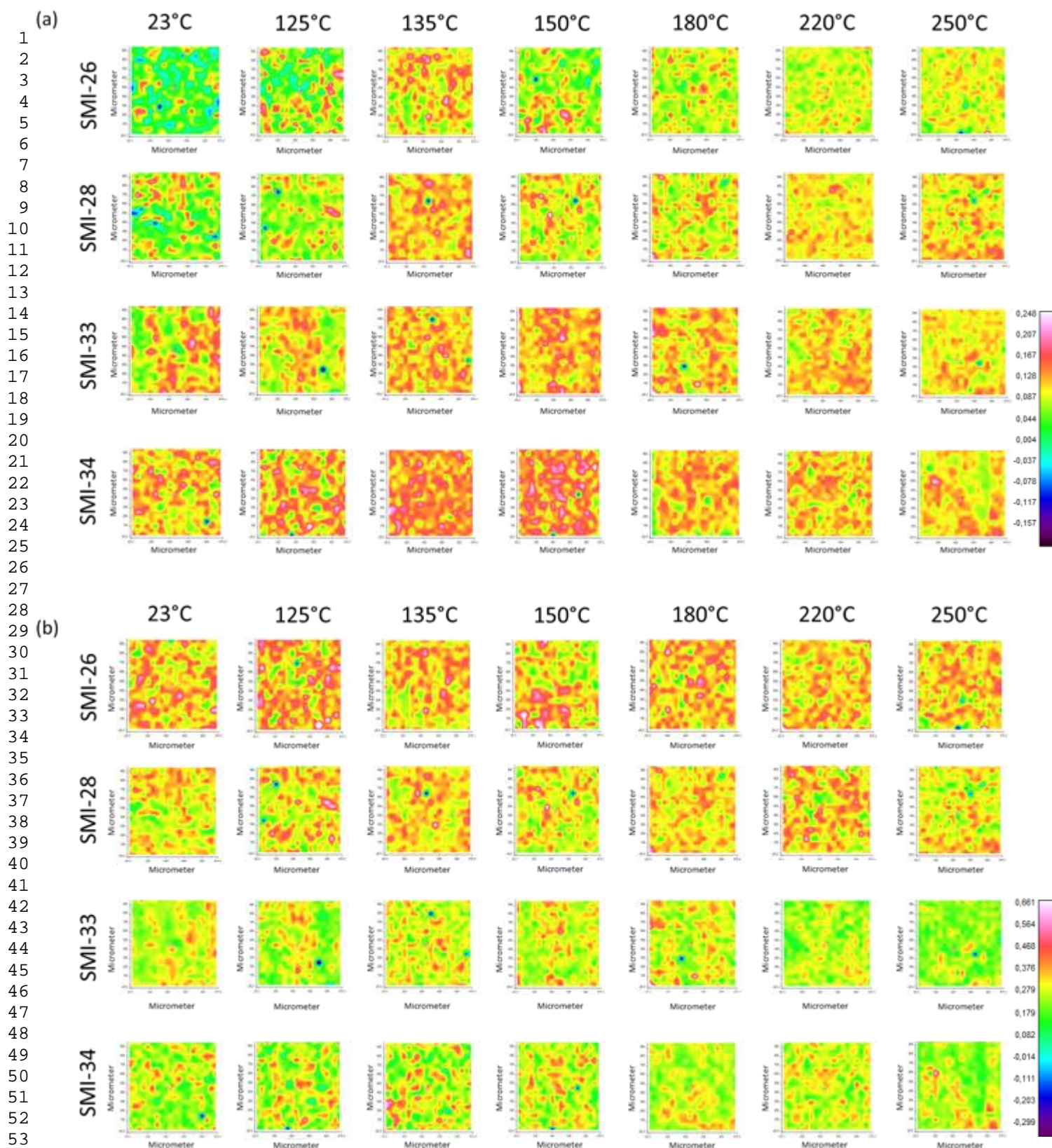
11

Figure 4. Raman surface maps (1 x 1 mm^2) for different coating grades after thermal curing at different temperatures: (a) band intensity ratio of imide (1785 cm^{-1}) / cellulose (1378 cm^{-1}), (b) band intensity ratio of styrene (1602 cm^{-1}) / cellulose (1378 cm^{-1}). Same intensity scale applies to all surface maps.

in intensities are noticed, the styrene intensities are evidently more comparable between SMI-26, SMI-28 (higher intensities) and SMI-33, SMI-34 (lower intensities) coating grades with small variations in composition, while they are more distinguishable between both subcategories. The imide intensities after thermal curing evolve to a maximum intensity at 135°C for the SMI-26 and SMI-28, and a maximum intensity at 150°C for the SMI-33 and SMI-34 coatings. At the higher temperatures, the imide coverage is more homogeneously spread over the surfaces in contrast with the low temperatures that include local imide deposits, characterized by single points in the surface maps with high intensity. This trend is in agreement with the previous analysis of the distribution of imide moieties within the coating itself (see **Figure 3**). The imide moieties are sensitive to thermal curing and ongoing reversion from ammonolyzed SMA (ring-opening reaction of maleic anhydride) into imide structure (ring-closing reaction by condensation). Therefore, the chemical surface mapping representing band intensity ratios seems to be sensitive to small variations in local surface compositions as well as sensitive to the overall surface composition of different coating grades.

The surface maps with intensities of single Raman bands are represented in **Figure 5**, where specific wavenumbers within the fingerprint region were selected corresponding to imide (1785 cm^{-1}), styrene (1602 cm^{-1}), cellulose (1378 cm^{-1}) and amic acid (1520 cm^{-1}). As an example indicating consistent trends and sensitivity of the Raman surface maps between different coating grades, the results for SMI-26 (**Figure 5a**) and SMI-33 (**Figure 5b**) are included. In contrast with the previous surface maps representing a band ratio, the surface maps with single bands were normalized (using the cellulose region 1170 to 1050 cm^{-1}) and baseline corrected in order to provide correct information. It can indeed be noticed that the locations with high intensities of single band imide coverage overlap with previous band ratio surface maps, while showing a maximum intensity at 135°C for SMI-26 towards 150°C for SMI-33. Also the comparison of relative intensity of the imide band for the different coating grades is representative with the higher values of maximum intensity for SMI-33 compared to SMI-26. The surface locations with single band styrene coverage coincide with the locations of imide coverage, both indicating the surface areas with high coating coverage, while the maximum intensities of the styrene band remains independent of the temperature and is higher for the SMI-26 compared to SMI-33. Although the relative intensity of the styrene band is also representative for the coating grades, it is not that pronounced compared to the imide band. The locations covered with high intensity of the single cellulose band are complementary to the locations with high intensity of imide and styrene bands, representing the presence of the paper substrate and lower coating coverage at those places. Mainly for the coating grades with higher
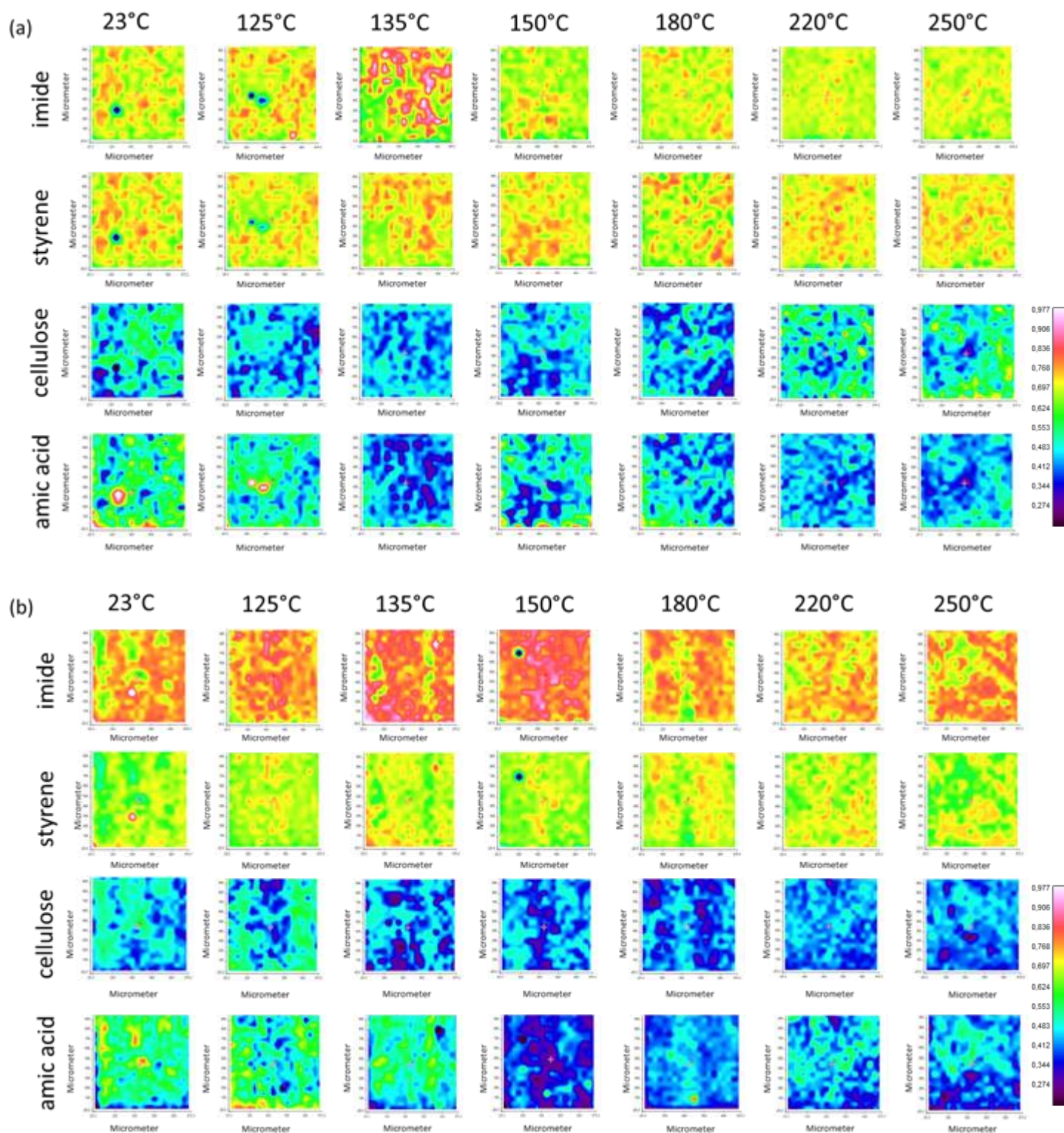
13

Figure 5. Raman surface maps (1 x 1 mm^2) with single band characteristic for imide (1785 cm^{-1}), styrene (1602 cm^{-1}), cellulose (1378 cm^{-1}), amic acid (1520 cm^{-1}), for two coating grades after curing at different temperatures, (a) SMI-26, and (b) SMI-33. Same intensity scale applies to all surface maps.

14

imide content, the maximum intensities of the cellulose band at the higher temperatures further diminish as the coating coverage becomes more homogenously spread over the paper substrate. Most interestingly, also the high intensities of the single band corresponding to amic acid is complementary to the imide coverage. As seen for the uncured coatings, local coating defects in imidization may be attributed to locally high concentrations of remaining amic acid originating from the ammonolyzed SMA precursor, which disappear after curing at higher temperatures. It is evident that the intensity of the amic acid band is minimized after thermal curing at 135°C (SMI-26) or 150°C (SMI-33), as the imidization is progressing in highest efficiency at those temperatures. The imidization reaction seems to be slightly reversible at the higher temperatures, where a slight decrease in imide intensities corresponds to a slight increase in amic acid intensities, relatively to the curing temperature of highest imide content.

A detail of the different Raman band regions attributed to the paper substrate (cellulose bands), is given in **Figure 6** in order to illustrate eventual interactions between the coating and the paper substrate. The surface maps for cellulose band regions at 1500 to 1220 cm^{-1} and 1220 to 1010 cm^{-1} are plot separately as band region maps, after similar baseline correction and normalization as before. Both cellulose band regions cover the same surface locations with high intensities and are complementary to the surface areas covered with high imide and/or styrene intensities, as they represent locations with a more pronounced presentation of the paper substrate and poor coating deposition. However, the intensity of the first cellulose region (C-C-H, O-C-H, H-C-H bending) is consistently lower compared to the second cellulose region (C-O-H, C-O-C stretching) at all locations, which reflect the influences of specific functional groups at the cellulose fibers. In particular, the higher intensity of bands related to C-OH stretching is due to the more pronounced presentation at the paper surface. The sensitivity of different cellulose functionalities to coating deposition is efficiently reflected in the surface maps that represent the intensities of the relative ratio of band regions (1220 to 1010 cm^{-1}) / (1500 to 1220 cm^{-1}) : it is remarkable that the locations with high intensity of this band ratio correspond to locations with high imide coverage from the coating according to previous single band surface maps. The intensity of the latter cellulose band region ratio also depends on the thermal curing temperature and intensifies in parallel with the previously noticed higher intensity for imide bands at 135°C (SMI-26) to 150°C (SMI-33). The intensity variation of the 1095 cm^{-1} band can also be noticed from the Raman spectra in previous Figure 2. Therefore, it is confirmed that the 1095 cm^{-1} cellulose band is sensitive to local reorganization around the C-OH cellulose functionalities during thermal curing and the interactions between the coating moieties and cellulose mainly occur through hydrogen bonding causing the more intense C-OH stretching.
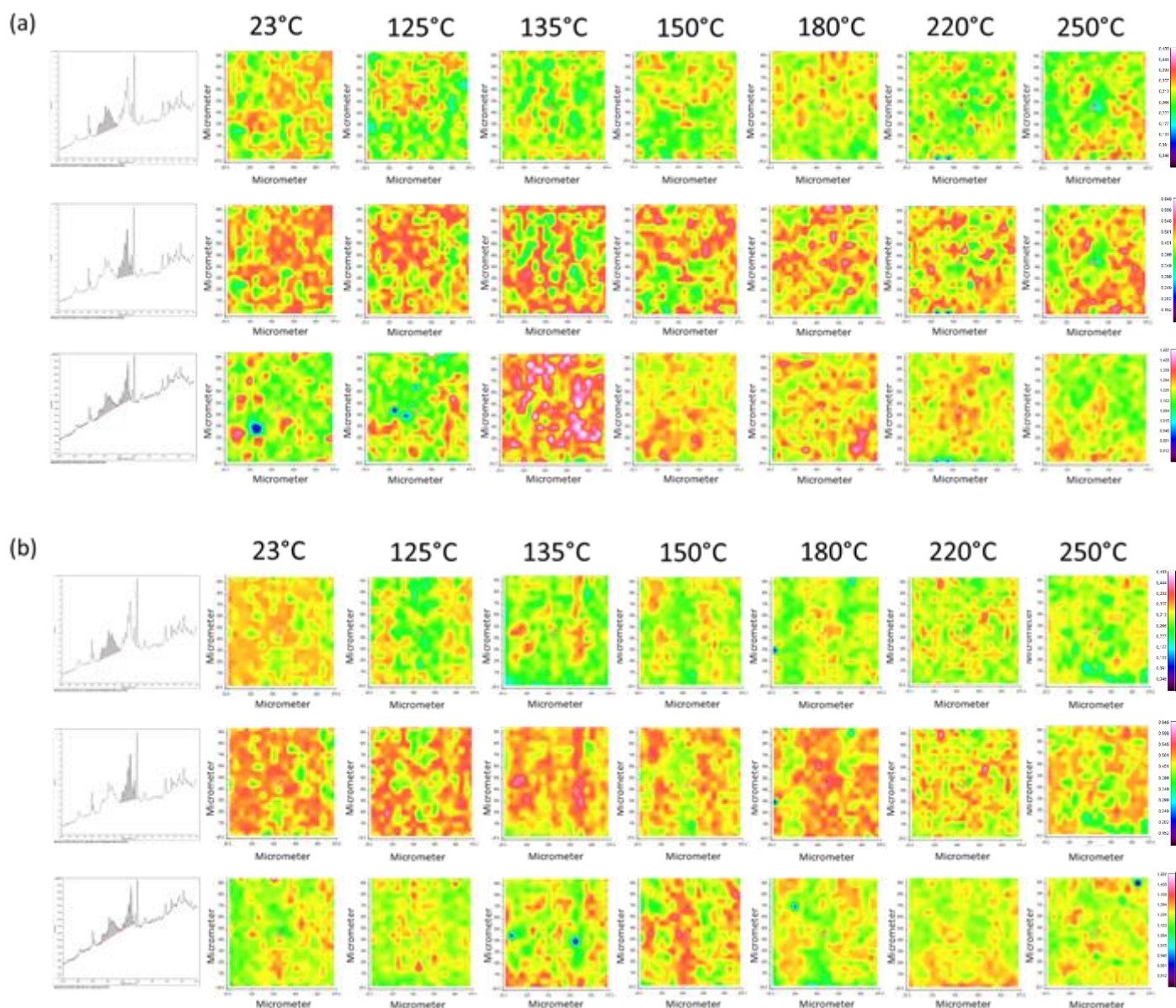
15

(a)

(b)

Figure 6. Raman surface maps (1 x 1 mm^2) with band ranges corresponding to cellulose (1500 to 1010 cm^{-1}) for two coating grades after curing at different temperatures, (a) SMI-26, and (b) SMI-33. Same intensity scale applies per line to all surface maps.

The surface maps with average intensities (or integrated area) of collected Raman spectra are represented in **Figure 7** for SMI-26 and SMI-33 coatings before and after thermal curing at different temperatures. The average intensity surface maps represent an average value of the full Raman spectra calculated at every point of the surface (after baseline correction and normalization as before), consequently including local information on the distribution of most prominent Raman bands. The average intensity maps are calculated according to a software procedure, where the original full spectral data with four dimensions (x (μm), y (μm), Raman

16

shift (cm^{-1}) and intensity) is reduced to three dimensions (x (µm), y (µm), intensity) by calculating the ordinate value as an average intensity value from the spectrum in each (x, y) coordinate point. In particular, it contains information related to certain chemical moieties and coating coverage, as illustrated below: it seems that the locations with high average intensities (yellow to red) correspond with the previously detected locations of coating deposits and locations with low average intensity (blue to green) correspond to poor coating deposits and more frequent presentation of the paper substrate, according to band ratio and/or single band surface maps. The average intensity surface maps are also sensitive to the coating grade, as the coatings with lower imide content (e.g., SMI-26) provide lower average intensities than to the coatings with higher imide content (e.g., SMI-33). Therefore, the average intensity surface maps include direct information on the coating coverage and imide content, consistently being highest after curing at 135°C (SMI-26) to 150°C (SMI-33) while the coverage at higher temperatures becomes more homogeneous.
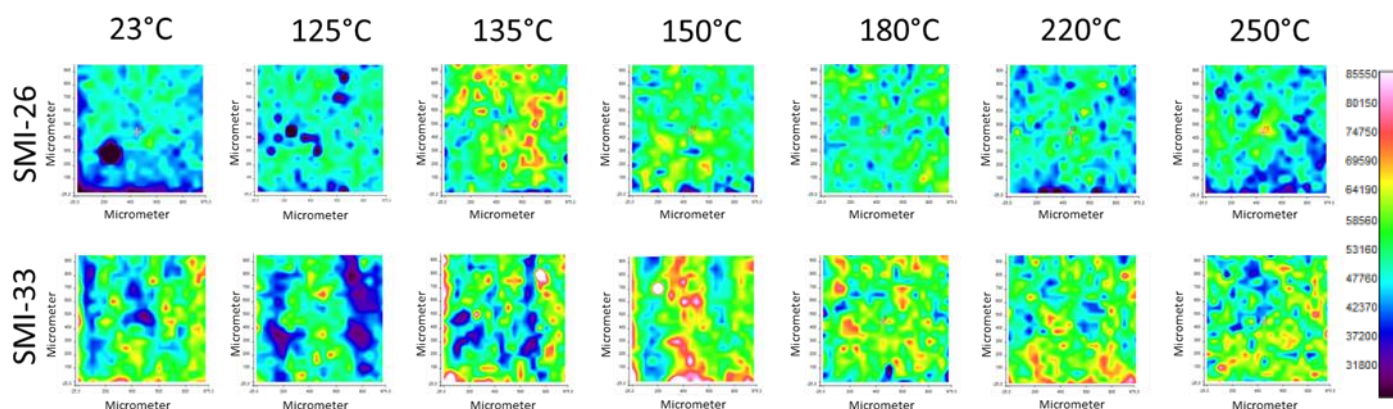

Figure 7. Raman surface maps (1 x 1 mm^2) with average intensity for two coating grades after curing at different temperatures, (a) SMI-26, and (b) SMI-33. Same intensity scale applies to all surface maps.

3.3 Principal component analysis

The most significant features in the spectra were extracted by using a basic analysis technique. In particular, the principal component analysis (PCA) is a statistical technique to find variations in a data set formed by the Raman spectra, by reducing the dimensionality by an orthogonal transformation of the original data set into a data set of values of orthogonal dimensions, so-called principal components (PC), where the largest amount of variances in the untransformed dimensions is represented in the first principal component (PC-1). The PC shows how the

intensity of Raman bands at different wavelengths change together and can be plot like spectra. As a result, the PCA searches for common factors that vary in the spectra and may come from variations between each measurement at a single location location (coating versus substrate) as well as from variations across the surface. A model for PCA of Raman spectra of coated papers was presently developed based on the analysis of a 2 class problem, by using two principal components (PC-1, PC-2) that were selected from a scree plot representing the percentage of residual variance for each component (PC-1: 82 %, PC-2: 16%), including 98 % of the total variance. The contributing variance for additional PC of a higher order was very small (< 2 %) and was consequently not further taken into account. In order to detect eventual outlier samples, the model has been based on a calibration set of samples with native and thermally cured coatings and was further validated by a leverage and residual analysis against PC-1 and PC-2 (data not shown): in conclusion, none of the included samples indicated simultaneous high leverage and high residue and should be considered as outliers.

The loading plots for PC-1 and PC-2 are shown in **Figure 8a**, as calculated from a set of Raman spectra by Unscrambler 10.1 software (see experimental details). The meaning of each PC can be recognized relatively to the original Raman spectra as follows: (i) the first factor PC-1 has prominent features for the coating moieties including characteristic Raman bands for imide and styrene, while (ii) the second factor PC-2 has prominent features for the paper base substrate including characteristic Raman bands for cellulose. Although the principal components are determined from a purely statistical analysis of the data set, they indeed provide good agreement with a consistent physical interpretation of the present data set. Some regions of Raman bands do not show overlap between coating and paper substrate for the Raman band at 1785 cm^{-1} (imide) and 1602 cm^{-1} (styrene), while the overlap in Raman bands between coating and substrate is efficiently discriminated in the PC-1 and PC-2, i.e. the Raman bands at 1452 cm^{-1} and 1200 to 1000 cm^{-1} (styrene overlap with cellulose) occur in either PC-1 or PC-2. Although the principal components are determined from a purely statistical analysis of the data set, the loading graphs of both principal components PC-1 and PC-2 are significantly different and provide a consistent physical interpretation of the present data set, which allows for a consistent analysis of the present system by the developed PCA model.
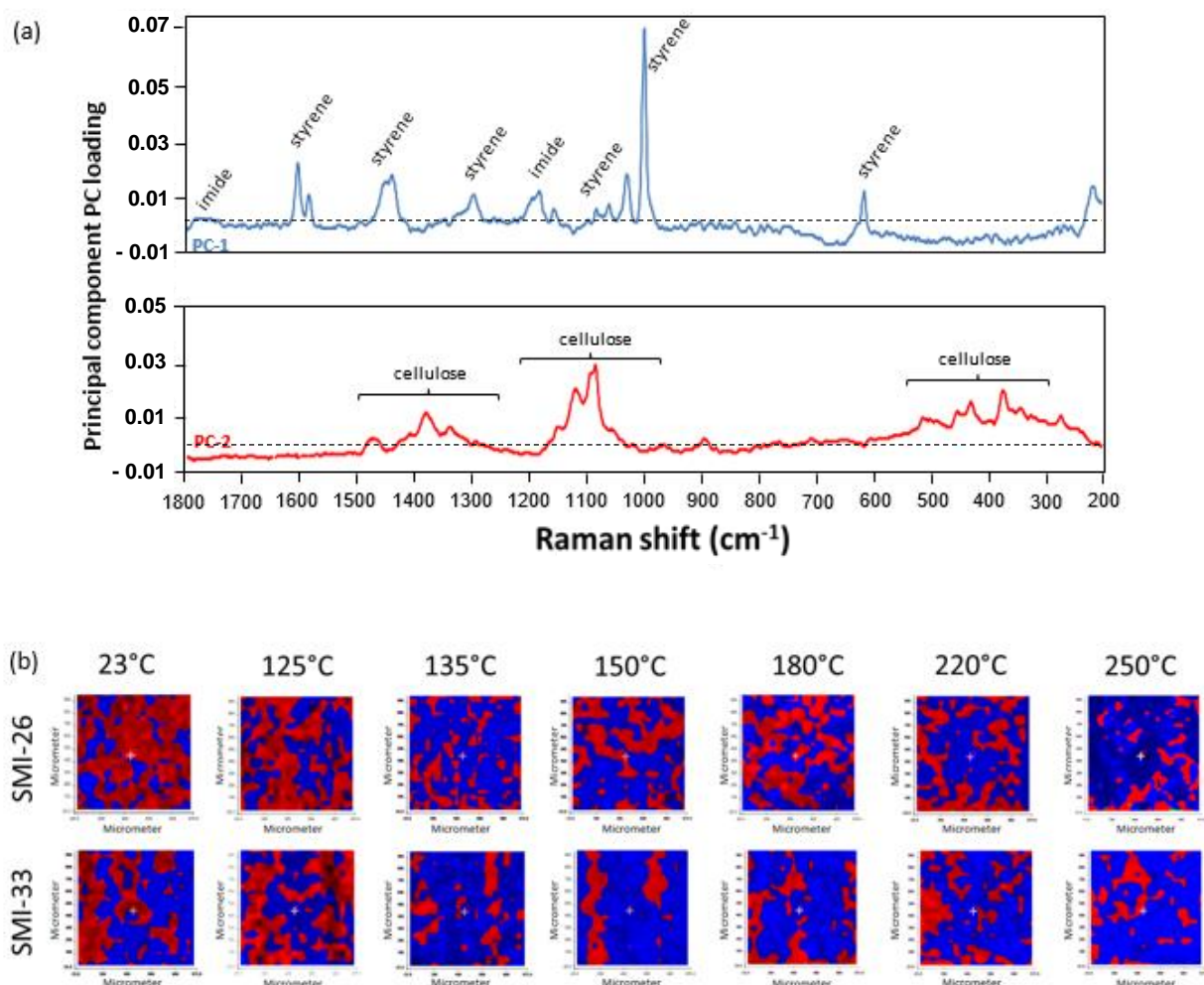
Figure 8. Principal component analysis (PCA) of Raman spectra for SMI coatings on paper, (a) loading plots for principal components PC-1 (coating) and PC-2 (paper) calculated by Unscrambler 10.1 software, (b) surface maps of PC-1 (blue) and PC-2 (red) for two coating grades after curing at different temperatures calculated by Spectrum Image R1.7 software.

The surface maps of both PC-1 and PC-2 for different coating grades were calculated by structural analysis of the original band intensity ratio Raman surface maps (1 x 1 mm^2) by Spectrum Image software (version R1.7, Perkin Elmer). The PC-1 and PC-2 surface maps for SMI-26 and SMI-33 coatings at different curing temperatures are shown in **Figure 8b,** indicating the locations on the paper coating surface corresponding with PC-1 (blue) or PC-2 (red) and further allowing to calculate a quantitative surface coverage (%) for each component. The surface maps with simultaneous coverage of PC-1 (coating) and PC-2 (paper) show good complementary between both PCs and can be compared against previous analysis of surface maps with band intensity ratio and/or single bands. The locations covered with high intensity

19

of band intensity ratios imide/cellulose or styrene/cellulose correspond to locations with high intensity of PC-1 (blue), confirming its physical representation of coating spectra. The surface coverage of PC-1 obviously increases with coating grade and has a maximum at curing temperatures of 135°C (SMI-26) to 150°C (SMI-33). The locations covered with high intensity of the cellulose bands correspond with the high intensity of PC-2 (blue).

3.4 Quantification

In addition to previously described qualitative observations from Raman spectra and chemical surface mapping, quantitative analysis of Raman spectra was made after a five-point calibration against a standard series of SMI grades with known imide content, i.e. 22, 26, 28, 33 and 34 mol-% respectively. The materials were obtained after imidization of corresponding grades of the SMA precursor with an excess of ammonium hydroxide relatively to the amount of maleic anhydride, i.e. ratio ammonium to maleic anhydride of 2.0 in contrast to the used SMI grades for coating applications that were imidized with a ratio ammonium to maleic anhydride of 1.01. As a result of complete imidization of the SMA, the imidized materials precipitated as a separate phase in the aqueous environment and were not obtained as a homogeneous aqueous dispersion of nanoparticles. This reflects the importance of the imide content of SMI nanoparticles used in coating applications and deposited from aqueous dispersion, which were intentionally not fully imidized as a remaining fraction of ammonolyzed maleic anhydride provides a negative charge around the nanoparticles and is responsible for charge stabilization of the SMI nanoparticle dispersions (zetapotential values $\zeta < -30$ mV, see **Table 1**). After filtration of the fully imidized materials and drying, they were used as reference materials for a calibration of the imide content relatively to specific Raman bands: in particular, a calibration curve was made with the imide content against the ratio of integrated intensities of the Raman band of imide (1785 cm^{-1}) relatively to styrene (1602 cm^{-1}), providing a relationship with statistical variance $R^2 = 0.996$ (**Figure 9**). By using this calibration method, the imide content is expressed relatively to the styrene content and represents the maximum imide content per coating grade, i.e. 26 / (100-26) = 35.1 % for SMI-26, or 28 / (100-28) = 38.8 % for SMI-28, or 33 / (100-33) = 49.3 for SMI-33, or 34 / (100-34) = 51.5 % for SMI-34. The calibration model was further confirmed by supplementary imidisation reaction for a copolymer SMA-22 (not used for coating applications), corresponding to a maximum imide content of 22 / (100-22) = 28.2 %. Therefore, the Raman spectra are sensitive to small variations in imide content and can

efficiently be used for further quantification of the imide content in the SMI nanoparticle coatings from the ratio of imide to styrene bands.
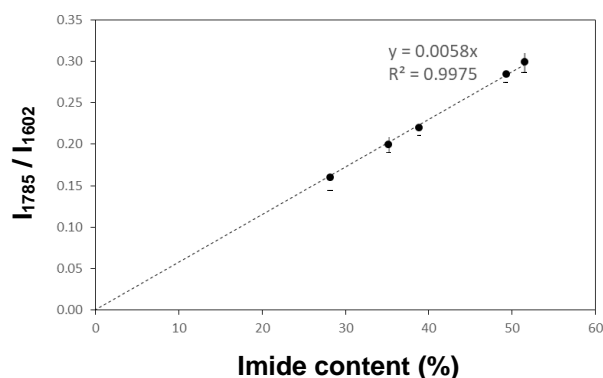

Figure 9. Calibration model for Raman band ratio I_{1785} / I_{1602} relatively to the imide content of synthesized poly(styrene-*co*-maleimide) or SMI grades with known imide content.

The calculated imide content from Raman spectra of the different coating grades after thermal curing at different temperatures is given in **Figure 10a**. The imide content was averaged from 10 different point measurements on the coated paper and represented as an average value with a statistical variation of about ± 0.3 %. The imide content of the coatings without thermal curing is, respectively, 25 % for SMI-26, or 33 % for SMI-28, or 40 % for SMI-33, or 45 % for SMI-34. It is indeed confirmed that the maximum imide content of the coatings without thermal curing is not attained. This is in agreement with the previous representation of surface maps with single bands of amic acid moieties corresponding to an amount of non-imidized and ammonolysed maleic anhydride. The imide content increases with curing temperature towards a maximum value at 135°C (SMI-26, SMI-28) to 150°C (SMI-33, SMI-34), while the imide content consistently increases progressively with coating grade. However, the maximum imide content was not obtained after thermal curing in none of the coatings: this can be explained through the interaction of the non-fully imidized SMI nanoparticles through hydrogen bonding with the cellulose fibers and hindering full imidizidation of the ammonolyzed (ring-opened) maleic anhydride. The maximum imide content and decline in imide content at higher temperatures illustrates that there is a thermodynamic optimum for the thermal curing process. In parallel, the surface coverage for the principal component PC-1 (coating) could be quantified from the surface maps (see previous Figure 8b) and is plot for the different coatings after thermal curing in **Figure 10b**. The surface coverage for each component is expressed as a percentage of the 1 x 1 mm^2 surface area that is covered by PC-1 and can be calculated from the surface maps by using the Spectrum Image software (version R1.7, Perkin Elmer). The

surface coverage for PC-1 (i.e., not the value of PC-1 as discussed later) follows a trend of increasing surface coverage with coating grade and a first maximum in surface coverage at
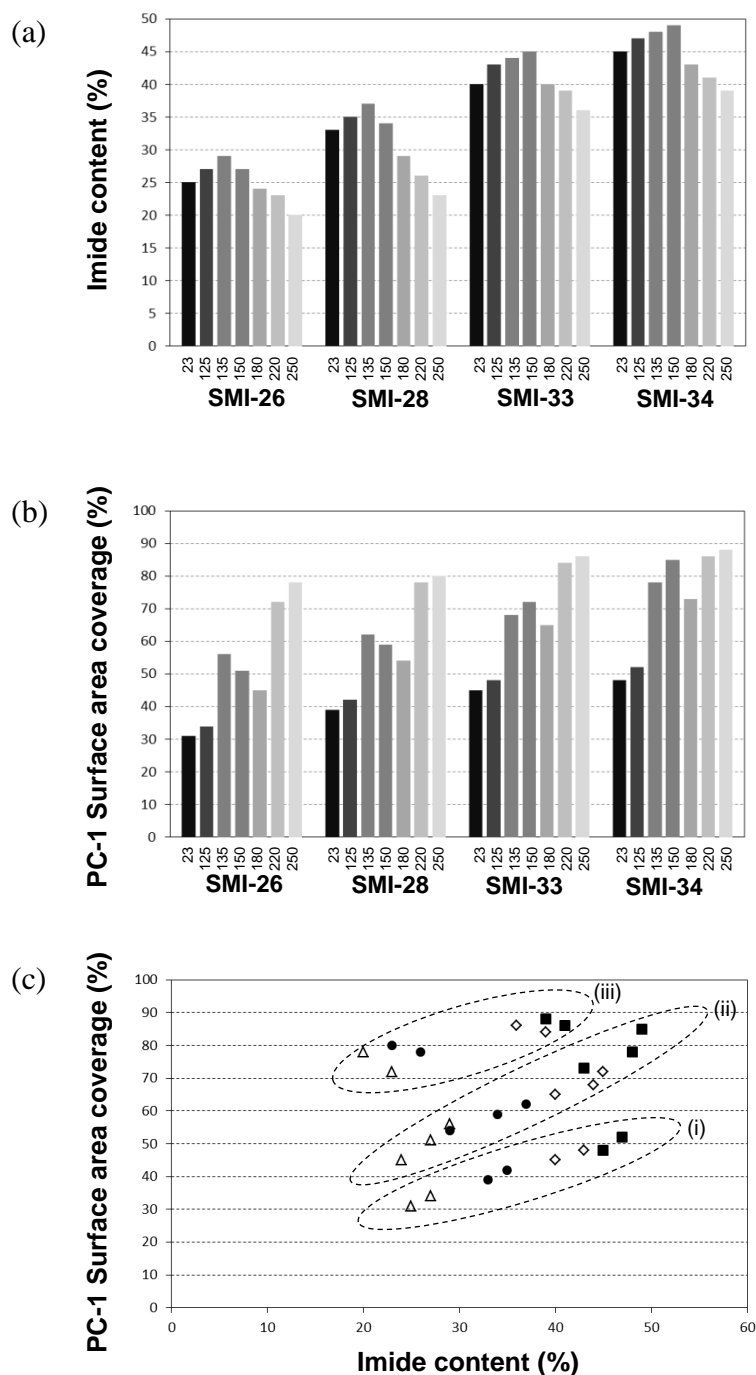

Figure 10. Quantification of Raman spectra and Raman mapping for different coating grades after thermal curing, (a) calculated imide content, (b) calculated surface coverage of PC-1, (c) relation between surface coverage of PC-1 and imide content for (Δ) SMI-26, (●) SMI-28, (◊) SMI-33, (■) SMI-34, regimes (i), (ii), (iii) see text.

135°C (SMI-26, SMI-28) to 150°C (SMI-33, SMI-34). At the higher temperatures above the glass transition temperature T_g of the coatings ($T_g = 180$°C), i.e. 220 to 250°C, the coating flattens and induces a larger surface coverage for PC-1 as the coating becomes more continuous over the surface through thermal softening (compare with SEM analysis, Figure 1d). From these values, a direct relation between the surface coverage for PC-1 and the imide content is plot in **Figure 10c**, indicating various trends depending on the temperature region grouped according to (i) non-cured and temperatures up to 125°C, (ii) temperatures 135 to 180°C, (iii) temperatures 220 to 250°C, as indicated in the graph. The latter gives good physico-chemical insight in the effect of different curing temperature regimes and indicates that the surface coverage of PC-1 is related to the thermal behavior and chemical properties of the coating with small alterations at low temperature (100 to 125°C), a shift in characteristics within the temperature region of chemical imidization reaction (135 to 180°C), and above the glass transition temperature (220 to 250°C).

According to the present PCA model, including a data-set of 10 different Raman spectra per coating grade and curing temperature (after baseline correction and normalization), the scores of PC-1 (coating) and PC-2 (paper) were calculated and are represented as average values (i.e., one single value is represented for 10 measurements per sample for clarity) with a statistical variation of ± 2 % between the 10 measurements. The two-dimensional score plot of PC-1 versus PC-2 is given in **Figure 11a** for all coating grades and thermal curing conditions, with the values of PC-1 and PC-2 within the 95 % confidence interval as calculated from the mean between all samples. The PCA shows consistent clustering of the scores according to the used coating grade, with an increase in PC-1 corresponding to a decrease in PC-2 among all samples and good overlap in the relationship between different coating grades and curing temperatures. Therefore, the PCA model with PC-1 and PC-2 corresponds with a valid physical interpretation of the data set, where the effects of the coating layer are included in PC-1 and effects of the paper substrate are included in PC-2, in agreement with the previous Figure 8a. The correlation between PC-1 and PC-2 in Figure 11a suggests that a higher imide content for the different coating grades or after thermal curing (high PC-1 score) corresponds with a lower presentation of the paper substrate (low PC-2 score). The latter trend with lower PC-2 score can be interpreted as a less intense contribution of the paper substrate to the Rama spectra due to better surface coverage and better homogeneity of the coating. The explicit physico-chemical meaning of the principal components becomes most clear when directly relating the scores to the calculated imide content, showing that the PC-1 score is a direct measure for the imide content

23

(**Figure 11b**) and the PC-2 score represents lower amount of cellulose exposed at the surface as the imide content increases due to the better coverage (**Figure 11c**).
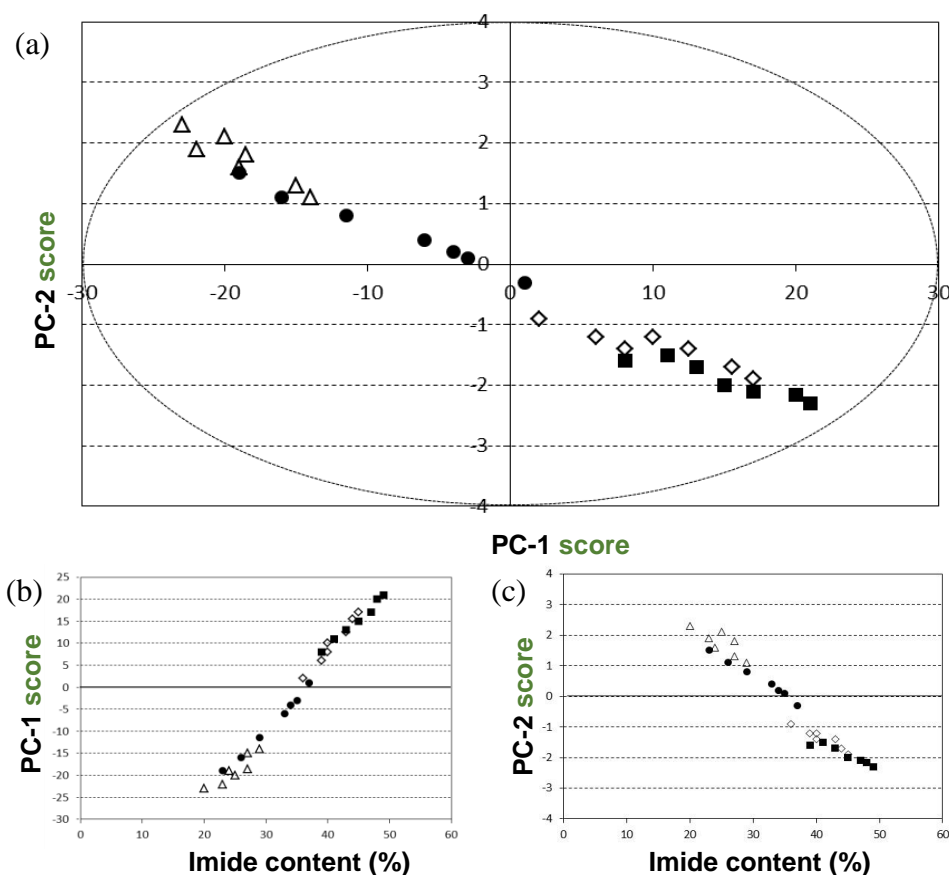

Figure 11. Quantification of PCA analysis: (a) score plot of PC-1 versus PC-2 with 95% confidence interval, (b) PC-1 versus calculated imide content, (c) PC-2 versus calculated imide content, for (Δ) SMI-26, (●) SMI-28, (◊) SMI-33, (■) SMI-34.

4. Conclusion

The Raman spectroscopy and confocal Raman mapping are favourable analytical tools to monitor variations in chemical surface composition for organic nanoparticle coatings on paper, in particular to detect local variations in chemical surface composition depending on the coating grade and thermal curing. For coating grades with variable content of functional imide groups, the coating coverage and variation in imide content at the surface can be qualitatively and quantitatively analyzed.

The Raman mapping shows an even distribution of the imide coatings on paper substrates with a maximum in imide content after thermal curing at 135°C (low imide grade coatings) to 150°C

24

(high imide grade coatings). Different regimes of thermal curing are observed at 100 to 125°C, 135 to 180°C and 220 to 250°C. The variation in imide content and reactivity of the coating during thermal curing is due to the further imidization of an amount ammonolyzed maleic anhydride, which is characterized by some specific Raman bands and occurs at locations that are complementary to the imidized parts of the coating. In parallel, the styrene content at the surface decreases with increasing imide content at the surface while it remains independent of the thermal curing process. There is good complementary in surface coverage of the Raman bands related to coating components and Raman bands related to the cellulose components. However, the variation in specific Raman bands for cellulose suggests that the interaction between the coating and cellulose fibers happens by hydrogen bonding. The principal component analysis on the present data-set of cured paper coatings can be applied with two principal components, corresponding to the variances of the coating (PC-1) and paper substrate (PC-2).

In conclusion, the variations in surface chemistry of the organic coating can be tuned by selecting specific ranges of curing temperatures and consequently allows for the alteration of resulting physical properties. The quantification of the surface chemistry is an important step in better understanding the response of the coating and can help as a tool for the design of functional surfaces.

References

[1] L.J. Douglas-Frink, J. Chem. Phys. **1999**, *110*, 5969.

[2] C.O. Ania, T.J. Bandosz, *Langmuir* **2005**, *21*, 7752.

[3] H. Woehlk, M.J. Trimble, S.C. Mansour, D. Pletzer, V. Trouillet, A. Welle, L. Barner, R.E.W. Hancock, C. Barner-Kowollik, K.E. Fairfull-Smith, *Polym. Chem.* **2019**, in press.

[4] L.K. Ista, M.E. Callow, J.A. Finlay, S.E. Coleman, A.C. Nolasco, R.H. Simons, J.A. Callow, G.P. Lopez, *Appl. Environ. Microbiol.* **2004**, *70*, 4151.

[5] H. Retsos, G. Gorodyska, A. Kiriy, M. Stamm, C. Creton, *Langmuir* **2005**, *21*, 7722.

[6] E. Detrait, J.B. Lhoest, B. Knoops, P. Bertrand, P.V.D. de Aguilar, *J. Neurosci. Methods* **1998**, *84*, 193.

[7] F. Guo, S.Y. Yang, C. Ma, P.L. Wong, *Tribol. Lett.* **2014**, *54*, 81.

[8] B. Bhushan, *Phil. Trans. R. Soc.* A **2009**, *367*, 1445.

[9] M. Nosonovsky, *Langmuir* **2007**, *23*, 3157.

[10] J. Jeevahan, M. Chandrasekaran, B. Joseph, R.B. Durairaj, M. Govindaraj, J. Coat. Technol. Res. **2018**, *15*, 231.

[11] J. Rull-Barrull, M. d'Halluin, E. Le Grognes, F.X. Felpin, Chem. Commun. **2016**, *52*, 2525.

[12] A. Arshad, H. Wang, X. Bai, R. Jiang, S. Xu, L. Wang, Spectrochim Act A **2019**, *206*, 16.

[13] R. Tankhiwale, S.K. Bajpai, *Coll Surf B B* **2009**, *69*, 164.

[14] H. Matsubara, M. Takada, S. Koyama, K. Hashimoto, K.; Fujishima, *Chem. Lett.* **1995**, *24*, 767.

[15] P. Samyn, *J. Mater. Sci.* **2013**, *48*, 6455.

[16] X. Wang, Z. Zheng, J. Wang, W. Chen, *Appl. Surf. Sci.* **2013**, *266*, 319.

[17] Q. Ha, L.Y. Liu, M.A. Karaaslan, S. Renneckar, *Front. Chem.* **2019**, *7*, 515.

[18] A. Geissler, F. Loyal, M. Biesalski, K. Zhang, *Cellulose* **2014**, *21*, 357.

[19] C.G. Obeso, M.P. Sousa, W. Song, *Colloids Surf A* **2013**, *416*, 51.

[20] V.K. Rastogi, D. Stanssens, P. Samyn, *Materials* **2014**, *7*, 7196.

[21] M. Poorteman, A. Renaud, J. Escobar, L. Dumas, L. Bonnaud, P. Dubois, M. Olivier, Prog. Org. Coat. **2016**, *97*, 99.

[22] S. Chen, H. Tanaka, *J. Wood Sci.* **1998**, *44*, 303.

[23] M. Stepien, J.J. Saarinen, H. Teisala, M. Tuominen, M. Aromaa, J. Haapanen, J. Kuusipalo, J.M. Mäkelä, M. Toivakka, *Langmuir* **2013**, *29*, 3780.

[24] J. Preston. In: *Advances in Pulp and Paper Research*, Trans. of the XIVth Fund. Res. Symp. Oxford, **2009**, 749.

[25] J. Qin, K. Chao, M.S. Kim, In: *Computer Vision Technology for Food Quality Evaluation*, Elsevier, **2016**, 141.

[26] M. Edinger, D. Bar-Shalom, J. Rantanen, N. Gennia, *Pharmaceut. Res.* **2017**, *34*, 1023.

[27] T. Kanbayashi, A. Ishikawa, M. Matsunaga, M. Kobayashi, Y. Kataoka, *Coatings* **2019**, *9*, 621.

[28] J.B. Cooper, *Chemom. Intell. Lab. Syst.* **1999**, *46*, 231.

[29] P. He, S. Bitla, D. Bousfield, C.P. Tripp, *Appl. Spectr.* **2002**, *56*, 1115.

[30] C. Kugge, M. Greaves, K. Hands, F.H. Scholes, N. Vanderhoek, J. Ward, *Appita* **2008**, *61*, 11.

[31] E. Pigorsch, M. Finger, S. Thiele, E. Brunner, *Appl. Spectr.* **2013**, *67*, 59.

[32] S. Bitla, C.P. Tripp, D. Bousfield, *J. Pulp Paper Sci.* **2003**, *29*, 382.

[33] P. Niemela, J. Sumen, J. Suhonen, Proceedings SPIE **2005**, *5826*, 406.

[34] J. Vyörykka, K. Juvonen, D. Bousfield, T. Vuorinen, Tappi J. **2004**, *3*, 19.

[35] P. Samyn, M. Deconinck, G. Schoukens, D. Stanssens, L. Vonck, H. Van den Abbeele,
Polym. Adv. Technol. **2012**, *23*, 311.

[36] U.P. Agarwal, *Molecules* **2019**, *24*, 1659.

[37] P.T. McKittrick, J.E. Katon, *Appl. Spectr.* **1990**, *44*, 812.

[38] N. Brun, I. Youssef, M.C. Chevrel, D. Chapron, C. Schrauwen, S. Hoppe, P. Bourson, A.
Durand, *J. Raman Spectr.* **2013**, *44*, 909.

Table of Contents.

Raman spectroscopy and chemical imaging by confocal Raman microscopy has been applied to detect the variation in chemical moieties at the surface of coated papers as a function of the thermal curing temperature. The combination with principal component analysis allows to derive qualitative and quantitative data on surface coverage and imide content.

Keyword surface characterization

P. Samyn,* W. Marchal, D. Vandamme, P. Adriaensens, and R. Carleer

Monitoring variations in thermal curing of nanoparticle coatings through confocal Raman microscopy and principal component analysis